Available online at www.sciencedirect.com
SCIENCE DIRECT
Marine and Petroleum Geology 23 (2006) 605–619
Marine and Petroleum Geology
www.elsevier.com/locate/marpetgeo

Mineralogical and geochemical characterization of hydrocarbon seep sediments from the Gulf of Mexico

Carles Canet[a,*], Rosa María Prol-Ledesma[a], Elva Escobar-Briones[b], Carlos Mortera-Gutiérrez[a], Rufino Lozano-Santa Cruz[c], Carlos Linares[a], Edith Cienfuegos[c], Pedro Morales-Puente[c]

[a]*Instituto de Geofísica, Universidad Nacional Autónoma de México, Ciudad Universitaria, Coyoacán 04510, México, D.F.*
[b]*Instituto de Ciencias del Mar y Limnología, Unidad Académica Sistemas Oceanográficos y Costeros, A. P. 70-305 Ciudad Universitaria, Coyoacán 04510, México, D.F.*
[c]*Instituto de Geología, Universidad Nacional Autónoma de México, Ciudad Universitaria, Coyoacán 04510, México, D.F.*

Received 22 September 2005; received in revised form 5 May 2006; accepted 11 May 2006

Abstract

A common characteristic of the Gulf of Mexico (GOM) seafloor, hydrocarbon seepage produces asphalt volcanism, brine pools, gas hydrates and authigenic carbonates. We studied authigenic carbonates from two areas: Green Canyon (Louisiana slope, 1000 mbsl) and the Chapopote diapir (abyssal plain, southwestern GOM, 2900 mbsl). Carbonates consist of oily, matrix-supported limestones with variable porosity and a fine-grained matrix of calcite. They occur in Green Canyon as both concretions formed below the seafloor and as slabs of seabed pavements. In each case, the carbonates are mudstones with a mud matrix consisting of high-Mg calcite, disseminated pyrite and detrital quartz. The carbonate slabs have vug microporosity and contain barite that occurs as vug lining. The precipitation of barite results from a reaction between barium-rich and sulfate-free seep fluids and downwards-diffusing seawater. The carbonates in Chapopote occur in relation to tar flows and form crusts of wackestones with bivalve shells. The matrix is composed by low-Mg calcite with disseminated pyrite and detrital quartz. The carbonate mud shows depletion in ^{13}C, with $\delta^{13}C$ between −36.9‰ and −23.0‰. Carbonates precipitate as a consequence of anaerobic methane oxidation coupled with seawater sulfate reduction. $\delta^{18}O$ values (3.4–4.4‰) suggest precipitation at temperatures between 5 and 9 °C.

Keywords: Cold seeps; Carbonates; Barite; Stable isotopes

1. Introduction

Seafloor hydrocarbon seepage produced by the persistent and rapid upward migration of oil and gas from deeper sediments toward the water column represents a significant source of fossil organic carbon in the ocean and atmosphere (e.g., Milkov et al., 2004). The discharge of hydrocarbons into the seafloor sediment at discrete areas known as cold seeps produces mud and asphalt volcanoes, brine pools, gas hydrates and deposits of authigenic minerals. It also sustains complex chemosynthetic communities. These characteristics have been reported in several other continental margins. Examples include the active subduction margins of Cascadia (Suess et al., 1999), the Costa Rica margin (Han et al., 2004), the Mediterranean Ridge (Aloisi et al., 2004), the Nankai Trough (Ashi et al., 2002), the Oregon–Washington margin (Ritger et al., 1987) and the active transform margin of Central California (Stakes et al., 1999). They are also featured in forearc basins related to island arcs, such as those in New Ireland, Papua New Guinea (Schmidt et al., 2002) and in the Barbados accretionary wedge (Lance et al., 1998). Cold seeps have been also widely recognized in the passive margins of the Black Sea (Peckmann et al., 2001; Michaelis et al., 2002), Baffin Island (Matsumoto, 1990), the Barents

*Corresponding author. Tel.: +52 55 56224133; fax: +52 55 55502486.
E-mail address: ccanet@tonatiuh.igeofcu.unam.mx (C. Canet).

0264-8172/$ - see front matter © 2006 Elsevier Ltd. All rights reserved.
doi:10.1016/j.marpetgeo.2006.05.002

Sea (Milkov et al., 2004), the Gulf of Cadiz (Pinheiro et al., 2003) and the northern Gulf of Mexico (GOM) (Joye et al., 2004; MacDonald et al., 2004).

Oceanic gas hydrates generally accumulate huge amounts of hydrocarbons, mainly methane (Collett and Kuuskraa, 1998). However, recent research suggests that their probable reserves have been greatly overestimated (Milkov, 2004) and associated hydrocarbon reserves have proven even more difficult to evaluate. Methane flux currently being produced by seepage and gas hydrate destabilization likely represents a significant contribution to the global methane budget (e.g., Luff et al., 2004). Consequently, the potentiality of cold seeps as energy source and their effect on climate change has attracted the attention of the scientific community (e.g., Hovland and Judd, 1988; Judd et al., 1997; Collett and Kuuskraa, 1998). The practice of identifying methane-related carbonates on the seafloor as a key to exploring buried hydrocarbon reservoirs has been employed in the GOM by PEMEX, Mexico's national oil company (Pacheco-Muñoz et al., 2005). The effectiveness of the method is also supported by results obtained in the South China Sea (Chen et al., 2005).

The seafloor hydrocarbon seeps in the GOM are, in effect, "leaks" from subsurface oil and gas fields (Sassen et al., 2001). Faults related to salt tectonics (Macgregor, 1993) facilitate the rise of hydrocarbons from these oil and gas reservoirs to the seafloor. Thus, many of the cold seeps in the GOM are found on knolls and ridges created by the formation of salt domes (Bohrmann and Schenck, 2004). These cold seep sites have been associated with chemosynthetic life ecosystems and widespread deposits of gas hydrates and authigenic carbonates (e.g., MacDonald et al., 2004). In the Campeche Knolls in the southwest GOM, many lava-like flows of solidified asphalt have been described in close association to gas hydrate deposits and seepage of gas and oil (MacDonald et al., 2004).

In the GOM, types I and II gas hydrates mostly occur as deposits buried within the seafloor superficial sediments. They crop out locally as hydrate mounds forming detectable bathymetric features (MacDonald et al., 2003; Sassen et al., 2004). Forming and destabilizing according to the continuously fluctuating temperature of seawater near the ocean bottom (MacDonald et al., 2003), these deposits support complex benthic communities. These include colonies of "Methane ice worm" annelids (Fisher et al., 2000) and chemosynthetic seep microbial communities that anaerobically oxidize hydrocarbons and reduce seawater sulfate (Aharon and Fu, 2000).

The microbially mediated reactions that take place in cold seeps increase carbonate alkalinity and sulfide activity, resulting in the formation of authigenic mineralizations essentially comprised of calcium carbonates (calcite, high magnesium calcite, aragonite and dolomite) (e.g., Wallmann et al., 1997; Stakes et al., 1999; Aloisi et al., 2000; Peckmann et al., 2001; Aloisi et al., 2004). Their precipitation is attributed to the coupled reaction of the bacterial reduction of seawater sulfate and the oxidation of discharged methane (Ritger et al., 1987). This increases the alkalinity of the environment and the water saturation state with respect to carbonate minerals (Peckmann et al., 2001). The generated sulfide reacts with iron of the detrital minerals to produce pyrite (Peckmann et al., 2001). The processes of carbonate precipitation with associated pyrite as triggered by microbial activity have been widely reported in many cold seeps and even in hydrothermal methane-rich submarine vents (Canet et al., 2003). In some cold seeps, barite also precipitates as the barium-rich and sulfate-free cold seep fluids that are expelled react with sulfate-rich, downwards-diffusing seawater (e.g., Paytan et al., 2002; Torres et al., 2003; Aloisi et al., 2004).

Several fossil cold seep authigenic sediments have been recognized. For example, Cavagna et al. (1999) described Tertiary aged limestones derived from cold seeps in Monferrato, Italy. In Neuquén, Argentina, Gómez-Pérez (2003) described a Jurassic stromatolitic bioherm that was possibly of the same origin. Cold seep related carbonate deposits of Paleozoic age are extremely scarce (Peckmann and Thiel, 2004). However, the origin of some large stratiform barite deposits of Paleozoic age could be attributed to the expulsion of hydrocarbon, barium-rich cold seep fluids (Torres et al., 2003), despite evidence of certain formations clearly involving hydrothermal fluids (Emsbo and Johnson, 2004).

Microbially mediated reactions of methane oxidation at cold seeps serve as buffers for the release of methane into the oceans and the atmosphere. This characteristic along with the subsequent authigenic deposits have attracted the attention of the scientific community. However, detailed studies focused on the petrographic and mineralogical features of cold seep sediments are not as abundant as those taking a pure geochemical and biochemical approach.

In this paper we provide textural, mineralogical, chemical and carbon and oxygen stable isotopic data of modern cold seep authigenic carbonate deposits collected at two sites in the GOM. The first site was located in the Green Canyon area on the Louisiana slope and the other in the Campeche knoll area on an abyssal plain near the Campeche Bank (Fig. 1). We then examine the effects of the geological and environmental conditions on their formation.

2. The GOM: geological setting and environmental conditions

2.1. General setting

The GOM is a deep intercontinental sea located at the southeastern corner of North America. It covers an area in excess of 1.5 million km^2 and reaches a maximum water depth of approximately 3700 m. The gulf is a complex sedimentary basin that contains thick accumulations of detrital sediments and massive carbonates affected by complex salt tectonics (Roberts et al., 1999). Sediments

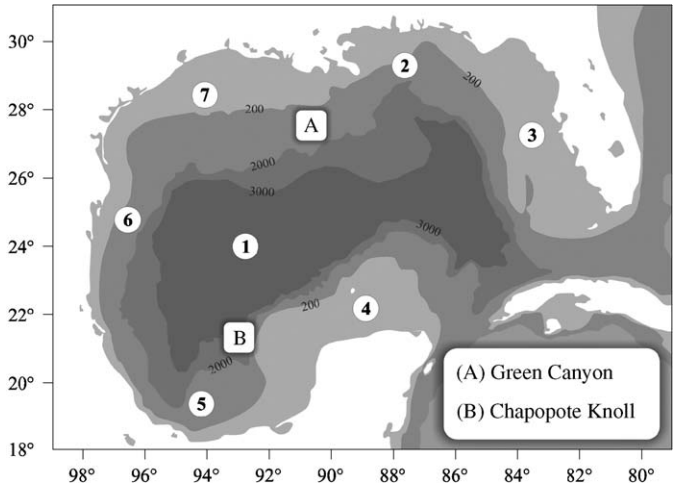

Fig. 1. Map of the Gulf of Mexico showing the location of the studied hydrocarbon seeps. Numbers indicate the geologic provinces established by Antoine (1972): (1) Gulf of Mexico Basin, (2) Northeast Gulf of Mexico, (3) South Florida Continental Shelf and Slope, (4) Campeche Bank, (5) Bay of Campeche, (6) Eastern Mexico Continental Shelf and Slope, and (7) Northern Gulf of Mexico.

from the Mesozoic to Cenozoic ages that have accumulated in the GOM attain a maximum thickness of nearly 15,000 m (Roberts et al., 1999).

Considered one of the world's most productive petroliferous basins, the GOM can be divided into seven geologic provinces according to Antoine (1972): (1) GOM Basin, (2) Northeast GOM, (3) South Florida Continental Shelf and Slope, (4) Campeche Bank, (5) Bay of Campeche, (6) Eastern Mexico Continental Shelf and Slope, and (7) Northern GOM (Fig. 1).

The central GOM basin includes the Mississippi Cone and the Sigsbee Abyssal Plain, a deep (more than 3000 mbsl) and extremely flat portion of the GOM bottom interrupted only by the large diapiric domes known as the Sigsbee Knolls (Ewing and Antoine, 1966).

In general, the shelves show smooth surfaces and the slopes are characterized by prominent escarpments, knolls, intraslope basins and submarine canyons (Roberts et al., 1999). Extensive and almost flat, the Campeche Bank is a carbonate bank that gradually changes to detrital sediments in the shallower waters of its western border (Antoine, 1972).

2.2. Geologic framework

In the area presently occupied by the GOM, the breakup of Pangea heralded a crustal extension phase in the Late Triassic that resulted in the local development of active grabens and rift basins (Salvador, 1987). A rifting event in the Middle Jurassic opened the GOM and precipitated oceanic spreading that began in the Late Jurassic period (Pindell, 1985). Thick evaporitic series were deposited after the early opening of the GOM (Pindell, 1985).

Accumulated in shallow hypersaline water bodies, salt deposits are generally deformed as a consequence of an intense diapirism and sediment accumulation. Although the precise dating of the salt deposits is uncertain, stratigraphic criteria suggest that they formed during the Callovian age in the Middle Jurassic (Salvador, 1987). The original thickness of the salt sequence is estimated to be between 3000 and 4000 m (Salvador, 1987).

After the opening of the GOM, a process of thermal subsidence that continued to the Early Cretaceous provided the accommodation space necessary to accumulate thick sedimentary sequences (Watkins and Macrae, 1995). Hence, Late Jurassic to Cenozoic sediments covered the salt deposits and created a thick continental margin sedimentary wedge. The eastward marine invasion started during the Oxfordian and ended during the Kimmeridgian (Late Jurassic), resulting in the connection of the GOM with the Atlantic Ocean (Salvador, 1987).

During the late Middle Jurassic and the early Late Jurassic, the Campeche Bank began to separate from the North American Plate due to seafloor spreading. Moving southward to its present position, its displacement resulted in the deepening of the central GOM and the separation of the Middle Jurassic salt deposits north and south of the Sigsbee Abyssal Plain (Salvador, 1987).

During the Cretaceous, the Campeche Bank was submerged and a sequence of mainly carbonates and evaporites was deposited (Morán-Zenteno, 1984). In the Yucatán Peninsula, this sequence is covered by an undeformed Tertiary calcareous sequence.

During Tertiary, intense salt diapirism deformed the overlying detrital sediments. Faults formed by salt tectonics intersected deep hydrocarbon reservoirs and allowed the upward migration of hydrocarbons to the seafloor (Sassen et al., 2001) and, in many cases, crop out at the seafloor that formed fault escarpments with associated slumps adjacent to cold seeps (Bohrmann and Schenck, 2004). The salt domes that cropped out above the seafloor formed submarine knolls and ridges.

2.3. Hydrographic and environmental conditions

The coastal surface waters of the GOM are characterized by strong influx from riverine freshwaters and strong evaporation rates (Tomczak and Godfrey, 1994). The offshore hydrodynamic conditions are dominated by the Loop Current to the east and large shedded anticyclonic rings to the west (Salas de León and Monreal-Gómez, 1997).

The physical and chemical conditions of water vary along the seawater column and define a surface layer, a thermocline and a deep layer (Fig. 2). The temperature ranges between 23 °C in the surface waters and 4 °C below 1500 mbsl and the salinity defines a halocline around 200 mbsl (Bohrmann and Schenck, 2004). The dissolved oxygen concentration in deep waters is high (Bohrmann and Schenck, 2004).

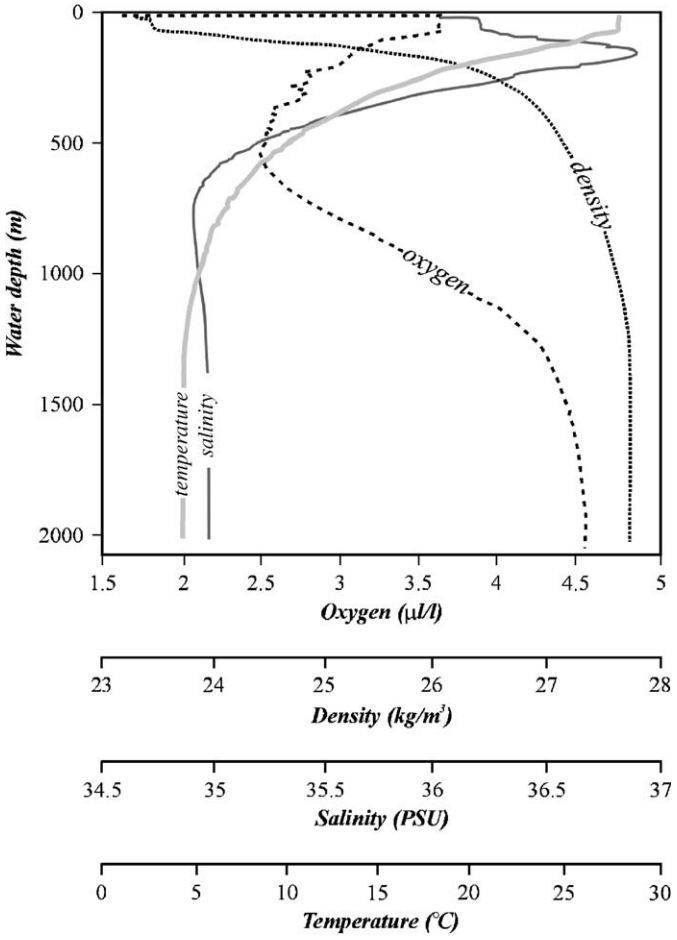

Fig. 2. CTD profile of the Green Canyon showing the variation of some hydrographic parameters along the seawater column (Bohrmann and Schenck, 2004).

3. Sampling and analytical methods

The analyzed samples were obtained during the SO-174 (OTEGA II) cruise of the German research vessel SONNE (1 October–12 November 2003). Rock samples were obtained with a TV-guided grab sampler and a gravity corer was used for sampling the unconsolidated sediments (for details see Bohrmann and Schenck, 2004).

Petrographic observations were made on thin polished sections of rock samples using an optical microscope. Thin polished sections were also analyzed with a Jeol JXA-8900R electron microprobe at the *Instituto de Geofísica* of the *Universidad Nacional Autónoma de México* (UNAM), allowing us to obtain back-scattered electron images, EDS qualitative analyses and WDS quantitative analyses of the carbonates. In addition, unpolished samples were examined at UNAM's *Instituto de Geología* using a Jeol JSM-35C scanning electron microscope (SEM) on secondary electron mode and operating at 20 kV.

X-ray diffraction (XRD) analyses were performed at UNAM's *Instituto de Geología* on a Philips 1400 diffractometer equipped with a Cu anode tube X-ray source and directing the collimated Cu $K_{\alpha 1,2}$ radiation ($\lambda = 0.15405$ nm) towards a randomly oriented sample. X-radiation was generated at 40 kV and 20 mA. Standard scans were recorded from 4° to 70° (2θ) with a step-scan of 0.02° and 2 s/step.

Whole rock chemical analyses were performed by X-ray fluorescence (XRF) at UNAM's *Instituto de Geología* using a Siemens SRS3000 sequential spectrometer. The samples were prepared as fused beads in a mix of $LiBO_2$–$Li_2B_4O_7$. To consult details about the sample preparation and the reference materials used to build the calibration curves, see Lozano-Santa Cruz et al. (1995).

Carbon and oxygen stable isotope analyses of carbonates were carried out at the LUGIS isotope laboratory of UNAM's *Instituto de Geología* using a Finnigan MAT 253 spectrometer. The mass spectrometry measurements were performed using a Finnigan Delta Plus XL with a dual inlet Gas Bench II interface with an autosampler GCPAL. The isotope ratio was determined simultaneously for carbon and oxygen using the Gas Bench II. All of the analyses were performed at 25 °C. For reference gas, we used CO_2 99.998% from a Praxair Tank ($\delta^{18}O_{VSMOW} = -7.16$ and $\delta^{13}C_{VPDB} = -11.29$) calibrated with an Oztech tank of CO_2 ($\delta^{18}O_{VPDB} = -9.78$ and $\delta^{13}C_{VPDB} = -10.99$). The results of $\delta^{18}O_{VPDB}$ and $\delta^{13}C_{VPDB}$ were normalized with NBS19 to scale VPDB according to Coplen (1988). To check the VPDB scale, we used NBS18 and LSVEC. The precision and accuracy of the whole set of samples was verified using a calcite reference sample which was analyzed every seven samples. The standard deviation reported for this technique is 0.2‰ for oxygen and 0.2‰ for carbon.

4. Description of the studied cold seep sites

The studied samples were collected from two different areas with cold seepage: (1) Green Canyon on the Louisiana slope in the northern GOM, and (2) Chapopote knoll on the abyssal plain near the Campeche Bank in the southwestern GOM (Figs. 1 and 3).

4.1. Green Canyon

The Green Canyon area is home to some of the most studied cold seeps in the GOM (e.g., Sassen et al., 2001, 2004; Aharon and Fu, 2003; Arvidson et al., 2004; Formolo et al., 2004). The seafloor topography shows a hummocky morphology characteristic of the entire Texas–Louisiana slope and formed as a result of salt diapirism (Bryant et al., 1991). Thus, the Multibeam Echosounder profiles obtained by Bohrmann and Schenck (2004) show rounded basins and salt domes that are a few kilometers in diameter, limited by fault scarps and scattered throughout the slopes. Faults related to diapiric structures serve as pathway for the upward migration of hydrocarbons to the seafloor and create numerous cold seeps.

We studied samples collected from two hydrocarbon seepage sites: (1) TVG-11, located at 27°33.48N/90°58.86W

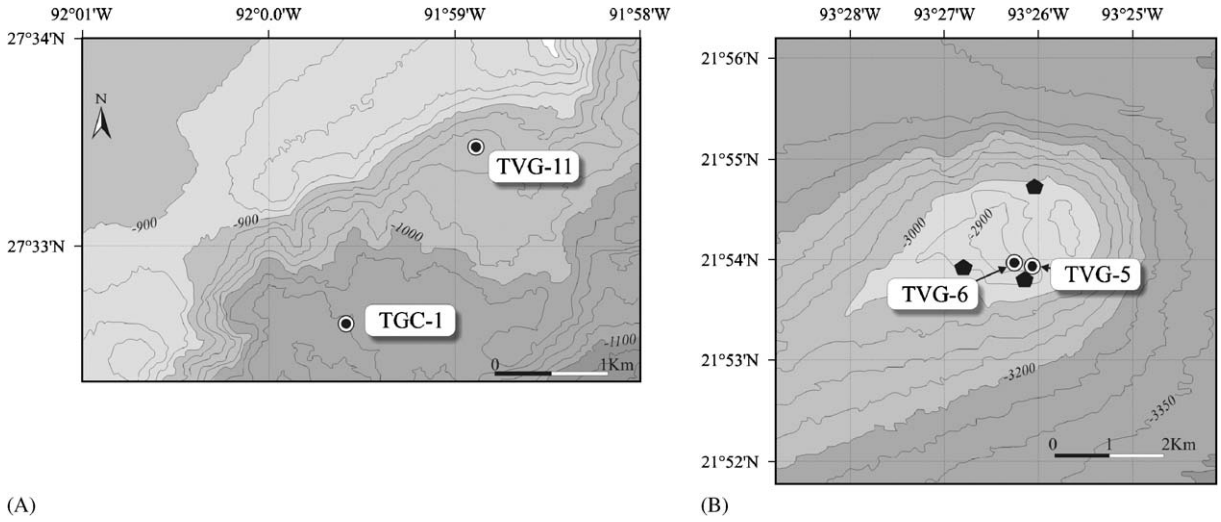

Fig. 3. Bathymetric maps of the studied hydrocarbon seepage areas showing the sampling sites: (A) Green Canyon, (B) Chapopote knoll. General location is shown in Fig. 1. After Bohrmann and Schenck (2004).

at a depth of 951 mbsl, and (2) TGC-1, located at 27°32.61N/90°59.54W at a depth of 1045 mbsl (Fig. 3A).

According to Bohrmann and Schenck (2004), the areas with cold seepage at the Green Canyon contain gas hydrate mounds, brine pools, oil slicks, authigenic carbonate deposits, shell beds and abundant benthic cold seep communities, with mussels, starfish, and small patches of sulfide oxidizing bacteria (*Beggiatoa*) mats.

Authigenic carbonates form hardground-like pavements and rocky outcrops scattered between nannofossil-rich, oily, muddy sediments. Locally, carbonate pavements with fossilized clam shells occupy extensive areas (Bohrmann and Schenck, 2004). Taking into account the gravity cores obtained by Bohrmann and Schenck (2004) around the TGC-1 seep site, the authigenic carbonates mostly form nodular and lens concretions below the water–sediment interface (Fig. 4). The sediment that hosts these carbonates is a nannofossil-rich, dark mud with strong H_2S smell. It also contains interlayered horizons of shell debris, patches saturated with oil and gas and gas hydrates forming disseminations and centimeter-thick veins. Pore waters have high H_2S concentrations and high alkalinity (Bohrmann and Schenck, 2004).

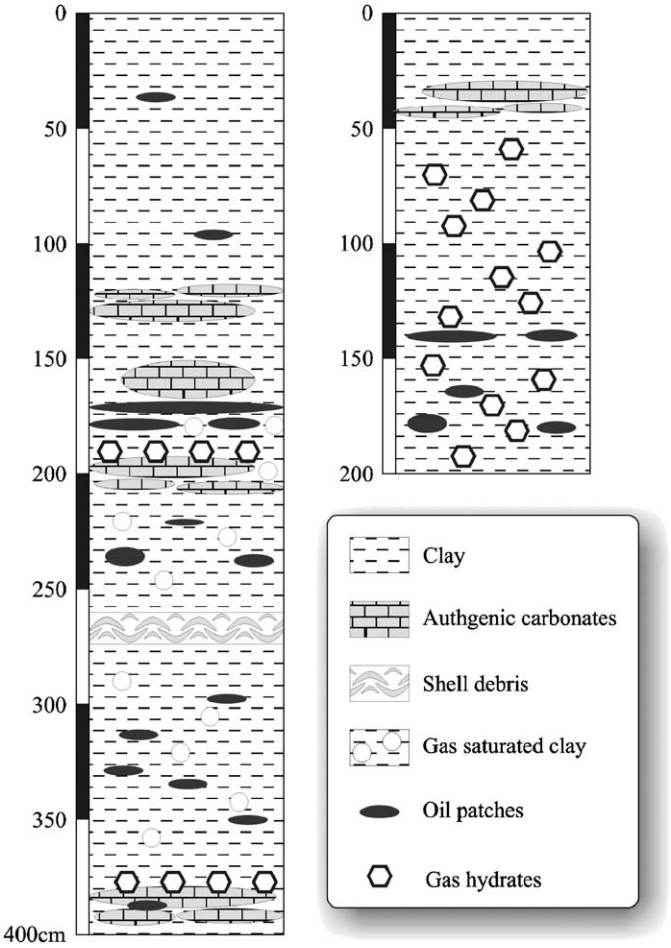

Fig. 4. Stratigraphic column of two cores obtained in the hydrocarbon seeps of the Green Canyon. After Bohrmann and Schenck (2004).

4.2. Chapopote knoll (Campeche knolls)

The Campeche knolls are a cluster of large salt domes located at the southern corner of the GOM basin abyssal plain near the Campeche Escarpment. These diapirs rise 450–800 m over an abyssal plain 3000–3500 m deep. They span up to 24 km in length and most of them are aligned northwest–southeast (MacDonald et al., 2004). In many cases, linear diapiric faults and crescent slumping scarps dissect the crests and flanks of the domes (MacDonald et al., 2004). Manifestations of persistent hydrocarbon seepage as oil slicks, cold seeps and asphalt volcanism are commonly associated to diapiric faulting in the salt domes (MacDonald et al., 2004).

The studied samples of authigenic carbonates and tar were collected in a fault dissected diapiric dome named by

MacDonald et al. (2004) as the Chapopote knoll. It is located at 21°54′N/93°26′W and reaches approximately 2900 mbsl at its summit (Fig. 3B). There, MacDonald et al. (2004) reported an intense asphalt volcanism that produced lava-like flow fields of solidified asphalt and rocky tar deposits often colonized by chemosynthetic fauna, including vestimentiferan tube worms and large *Vesicomyidae* and mussel bivalves. The tar outcrops are coated by bacterial mats and support communities of anemone, crinoids, shrimps, squat lobsters and holothurians (MacDonald et al., 2004). The abyssal sediments that surround the asphalt outcrops consist of nannofossil oozes, commonly show bioturbation and include tar boulders.

Authigenic carbonates form surface slabs and crusts associated with oil pools and anoxic H_2S rich sediments. The slabs and crust are colonized by tube worms and *Beggiatoa* mats (MacDonald et al., 2004). The samples of authigenic carbonates were collected in the TGV-6 sampling site located at 21°54.00′N/93°26.40′W at a depth of 2902 mbsl (Fig. 3B).

5. Hydrocarbon seepage-related sediments: petrographic characteristics and mineral chemistry

5.1. Hydrocarbon seeps in Green Canyon

Deposits of cold seep-related authigenic carbonates in Green Canyon appear as (1) concretions formed below the water–sediment interface, and (2) slabs forming hardground-like pavements. These carbonates are found in association to oily brown unconsolidated mud composed of clay minerals (illite, smectite), chlorite, quartz and minor calcite.

According to the Dunham (1962) classification, these carbonate concretions are mudstones. Decimeter-sized, they show a very irregular shape and develop macroscopic channel porosity that usually contains tar and oil (Fig. 5A and B). The microporosity, however, is very low and allochems are scarce (less that 5%) and supported by a matrix of carbonate mud.

Calcite and quartz are the only minerals detected by XRD analyses of bulk samples of the carbonate concretions, though minor amounts of pyrite and illite-like clay were identified using the optical and scanning electron microscope (Fig. 6). The position of the main XRD line $d(1\,0\,4)$ of calcite at 3.003 Å suggests that it is high-magnesium calcite.

The carbonate mud matrix is composed of calcite (Fig. 7) with minor amounts of quartz and pyrite. The EMP analyses of calcite crystals show $MgCO_3$ contents up to 9.99% molar, corresponding to high magnesium calcite in agreement with the XRD analyses (Fig. 8). Sodium and strontium are present in small quantities (up to 5193 ppm of Na and 2113 ppm of Sr) and values up to 680 ppm of barium have been analyzed.

Quartz forms randomly distributed silt-sized, rounded particles up to 30 μm in diameter and constitutes less that 1% of the fine-grained matrix. Pyrite occurs as fine-grained crystals about 5 μm in diameter scattered within the fine-grained carbonate matrix and inside the intraparticle and vug microporosity (Fig. 9A) associated with illite-like clay aggregates. The pyrite crystals are sometimes found as framboidal aggregates up to 250 μm in diameter (Fig. 6A).

The allochems are hyaline pelagic foraminifera with diameters up to 500 μm (Figs. 6 and 9). The foraminifer shells are composed by calcium carbonate with low magnesium between 0.30% and 1.14% $MgCO_3$ molar, moderately high sodium up to 9325 ppm and very low barium contents that are below detection limits. Strontium concentration ranges between 2249 and 2435 ppm.

The slabs of authigenic carbonates that occur as seafloor pavements around the cold seeps of the Green Canyon are approximately 5 cm thick and do not present channel macroscopic porosity (Fig. 5C and D). However, they do show abundant intraparticle and vug microporosity (Figs. 6B and 9B). According to Dunham's (1962) classification, the carbonate slabs are also mudstones, however, the volumetric percentage of allochems is higher than in the carbonate concretions described above.

Though calcite is the only mineral identified by XRD in the bulk samples from the carbonate slabs, minor amounts of aragonite, barite and pyrite were detected with optical and scanning electron microscopes. According to their magnesium concentration, the calcite crystals that compose the fine-grained matrix vary from high to low magnesium calcite and with barium levels reaching 349 ppm. Calcite forms a groundmass of short rhombohedral crystals approximately 10 μm in size (Fig. 7). Locally, the carbonate mud occurs as rounded intraclasts up to 500 μm in diameter. These are coated by a rim of aragonite cement and form aggregates with high intergranular porosity (Fig. 9B). The aragonite cement also rims some bioclasts and coats the vug porosity. Displaying a radial-fibrous fabric, the aragonite cement is composed of acicular crystals reaching 50 μm in length. With less than 0.1% $MgCO_3$ molar, these crystals are chemically low in magnesium (Fig. 8) and their barium content is below the detection limits. Their concentration of strontium ranges between 2376 and 2824 ppm.

Micron-sized single crystals of pyrite occur scattered within the carbonate mud but seldom arrange into small clusters or framboidal aggregates.

After calcite, the most common mineral is barite. It occurs in the carbonate slabs as a vug and crack lining and develops randomly oriented euhedral platy crystals up to 200 μm in length (Figs. 6C and 9C).

The allochems supported by the fine-grained matrix are rounded pelagic hyaline foraminifera with diameters up to 400 μm. The intraparticle porosity is usually filled by carbonate mud.

5.2. Hydrocarbon seeps on the Chapopote knoll

Seepage of hydrocarbons on the Chapopote knoll produces rocky-like deposits of solidified tar (Fig. 10) with

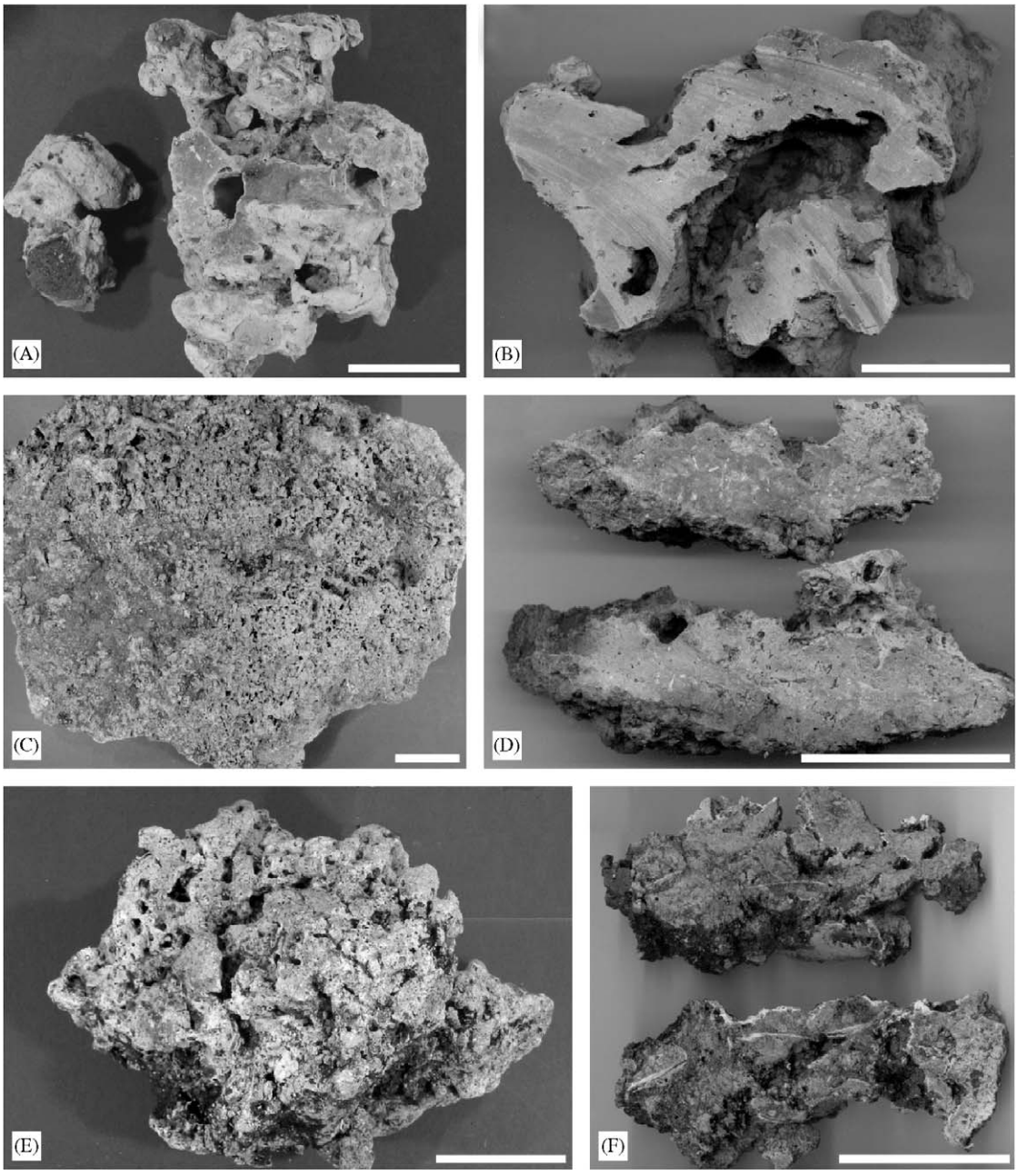

Fig. 5. Hand specimens of authigenic carbonates from hydrocarbon seeps in the Gulf of Mexico. Bar scale: 5 cm. (A) and (B) Subseafloor mudstone concretions with cavernous channel porosity from the Green Canyon. (C)and (D) Mudstone slabs from hardground-like seafloor pavements of the Green Canyon. (E) and (F) Porous wackestone rich in bivalve shell allochems associated with tar deposits from the Chapopote knoll.

associated slabs and crusts of authigenic carbonate (Fig. 5E and F). According to Dunham's (1962) classification, these carbonates are wackestones. They contain abundant bioclasts supported by a carbonate mud matrix and show high non-fabric-selective porosity and irregular vugs that vary significantly in size up to some millimeters. The rock is oily and its porosity is partly filled by tar. Acicular carbonate cement partially lines the porosity walls and binds allochems together.

Calcite, aragonite and quartz were detected by XRD analyses of the bulk samples. In addition, minor amounts of illite-like clay and pyrite were identified via the optical and SEMs.

The EMP analyses of calcite crystals that compose the fine-grained matrix show $MgCO_3$ contents up to 0.60% molar and correspond to low magnesium calcite (Fig. 8). With most values between 1500 and 2500 ppm, strontium contents are rather regular. However, barium content is erratic with analyses below the detection limits and values up to 599 ppm.

Detrital quartz grains a few microns in diameter are scattered throughout the carbonate mud matrix. Pyrite is

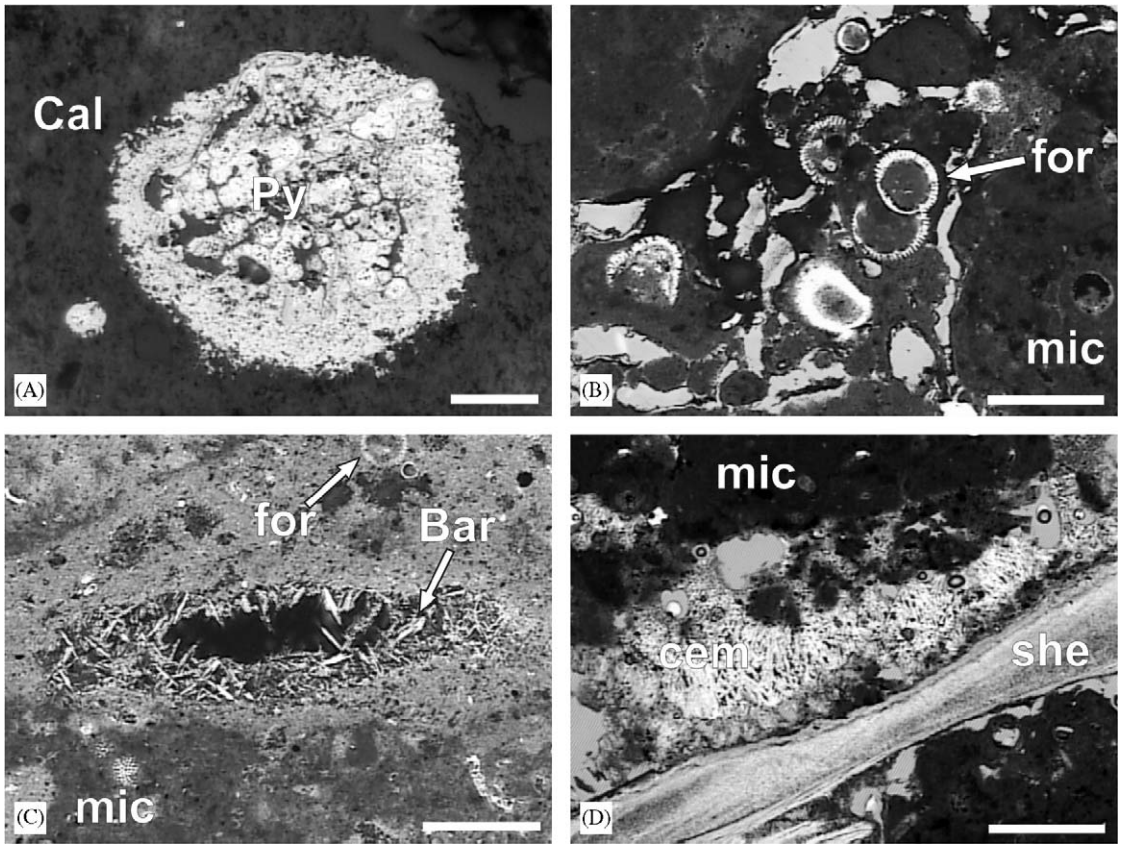

Fig. 6. Thin section micrographs of authigenic carbonates related to hydrocarbon seeps from the Gulf of Mexico. Bar, barite crystals; Cal, calcite crystals; cem, aragonite cement; for, foraminifer; mic, carbonate mud; Py, pyrite; she, bivalve shell. (A) Framboidal aggregate of pyrite contained in a fine-grained calcite matrix of a mudstone from the Green Canyon. Reflected light, bar scale: 50 μm. (B) Foraminifera in a seafloor mudstone slab of the Green Canyon. Plane polarized light, bar scale: 500 μm. (C) Vug filled by barite crystals in a seafloor mudstone slab of the Green Canyon. Plane polarized light, bar scale: 500 μm. (D) Bivalve shell cemented by aragonite acicular crystals in a wackestone from the Chapopote knoll. Plane polarized light, bar scale: 500 μm.

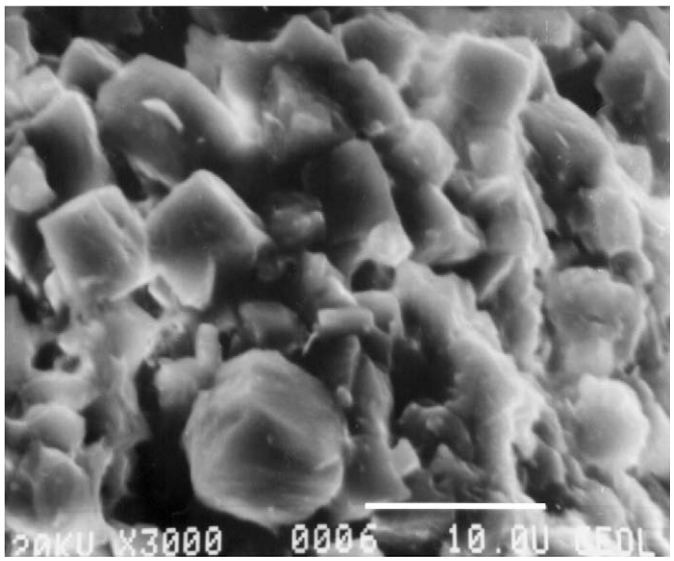

Fig. 7. Scanning electron microscope image on secondary electron mode of a mudstone concretion from the Green Canyon, showing an aggregate of rhombohedral crystals of calcite.

scarcer than in the Green Canyon carbonates. It occurs as micron-sized equant crystals scattered within the carbonate mud and, in larger amounts, within the porosity associated with illite-like, late infilling of clay (Fig. 9D).

Though the allochems are mainly bioclasts, some accumulation of intraclasts occurs near the vugs. The bioclasts are minor foraminifera and bivalve shells measuring up to several millimeters in length. Aragonite cement occurs in the vugs where it forms rims that line the porosity walls and bind the allochems (Figs. 6D and 9D). Aragonite develops acicular crystals that display radial-fibrous fabric and measure up to 500 μm length. These crystals have low magnesium contents up to 0.3% $MgCO_3$ molar. Strontium contents are rather regular with maximum values of 2401 ppm. The concentrations of barium and sodium reach 170 and 16758 ppm, respectively.

Illite-like clay occurs as a late-stage vug filling that partially occupies the porosity remaining after aragonite precipitation. It forms a greenish cryptocrystalline groundmass rich in fine-grained impurities and includes minor

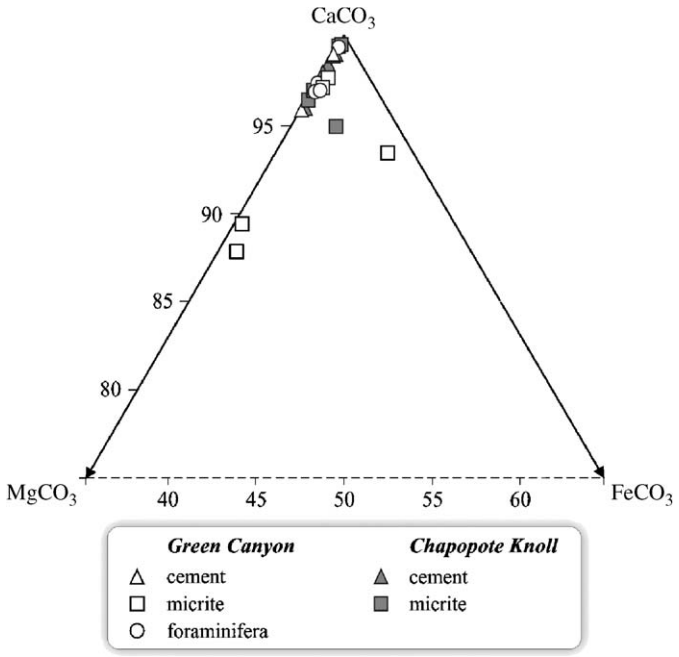

Fig. 8. Chemical composition of carbonate crystals from the hydrocarbon-seep-derived sediments of the Gulf of Mexico.

pyrite crystals (Fig. 9D). EDS qualitative microanalyses reveals that it has high K, Al and Si contents.

6. Whole rock chemical composition

Bulk rock chemical analyses of samples of hydrocarbon seep-related sediments are presented in Table 1. All the samples of authigenic carbonates show high CaO concentrations (between 36.6 and 42.9 wt%) in accordance with the predominance of calcite in the fine-grained matrix. Contrarily, the unconsolidated pelagic mud that hosts the carbonate deposits is poor in CaO (3.4 wt%) and rich in SiO_2 (51.3 wt%), consistent with the predominance of detrital quartz and sheet silicates. The latter are responsible for the high concentrations of iron and potassium.

Authigenic carbonates from seeps in the Green Canyon have high MgO concentrations with values between 3.4 and 4.2 wt%. These are in agreement with the high magnesium content of the calcite crystals that make up the carbonate mud. Samples also show significant barium enrichment. The Ba content varies between 239 and 280 ppm in the samples of carbonate concretions and reaches 4091 ppm in the carbonate slabs. This last value is consistent with the abundance of barite crystals found as vug filling in the carbonate slabs. In addition, barium content is also high in the unconsolidated mud (434 ppm). Conversely, the barium content in the authigenic carbonate deposits of the Chapopote knoll is much lower (33 ppm).

Vanadium and chromium contents are significantly high in the unconsolidated mud of the Green Canyon area at values of 220 and 96 ppm, respectively.

7. Stable isotopes

Fourteen stable isotopic analyses of carbon and oxygen were performed on bulk samples of cold seep carbonates from the GOM. Eleven of these analyses were carried out on mudstones from the Green Canyon; three on samples from the Chapopote knoll. With respect to the Green Canyon samples, we analyzed the mud matrix of both carbonate subseafloor concretions and slab pavements. Of the three Chapopote knoll sample analyses, two were performed on the mud carbonate matrix of the wackestone and one on an aragonite bioclast. The latter was analyzed as a reference. Stable carbon and oxygen isotopic analyses of calcite are summarized in Table 2 and Fig. 11.

The analyzed samples of carbonate mud show a strong depletion in ^{13}C with respect to normal marine carbonates. The $\delta^{13}C$ values range between −36.9‰ and −27.7‰ in the Green Canyon. In the Chapopote knoll samples, the carbonate mud is slightly less depleted in ^{13}C, with $\delta^{13}C$ values of −23.0‰ and −23.5‰. The analyzed aragonite bioclast—a bivalve shell—gives a $\delta^{13}C$ value of −3.7‰.

The $\delta^{18}O$ in carbonate mud of all the analyzed samples fluctuates within a narrow range of variation with values between 3.4‰ and 4.4‰. This range encompasses the oxygen isotope composition of the aragonite shell with its $\delta^{18}O$ value of 4.3‰.

There is no a clear correlation between $\delta^{18}O$ and $\delta^{13}C$. With respect to $\delta^{13}C$, the variation of $\delta^{18}O$ is slight and apparently independent (Fig. 11).

8. Discussion

8.1. Morphology and fabrics of carbonate deposits

Deposits of authigenic carbonates are a common feature of the hydrocarbon seeps of the GOM (e.g., Formolo et al., 2004; Sassen et al., 2004). These deposits display a variety of mineralogical and petrologic characteristics that show some variations between deposits—even within single deposits. In all the studied cases, fine-grained calcite builds matrix-supported, oil-impregnated limestones that contain variable amounts of bioclasts. Significant variations are shown in the type and volume of the porosity, the presence of late carbonate cements, the nature and abundance of the allochems and the morphology of the carbonate bodies. The chemical composition of the fine-grained calcite and accessory minerals also varies in these authigenic deposits.

In the hydrocarbon seeps of the Green Canyon, two morphological types of carbonates have been recognized: (1) concretions, and (2) slabs. The first occur a few meters below the water–sediment interface and show channel macroporosity. The second type form pavements containing vug microporosity and cover the seafloor. In the samples from the Chapopote knoll, bivalve-rich, irregularly shaped crusts occur in association with "rocky" submarine tar outcrops.

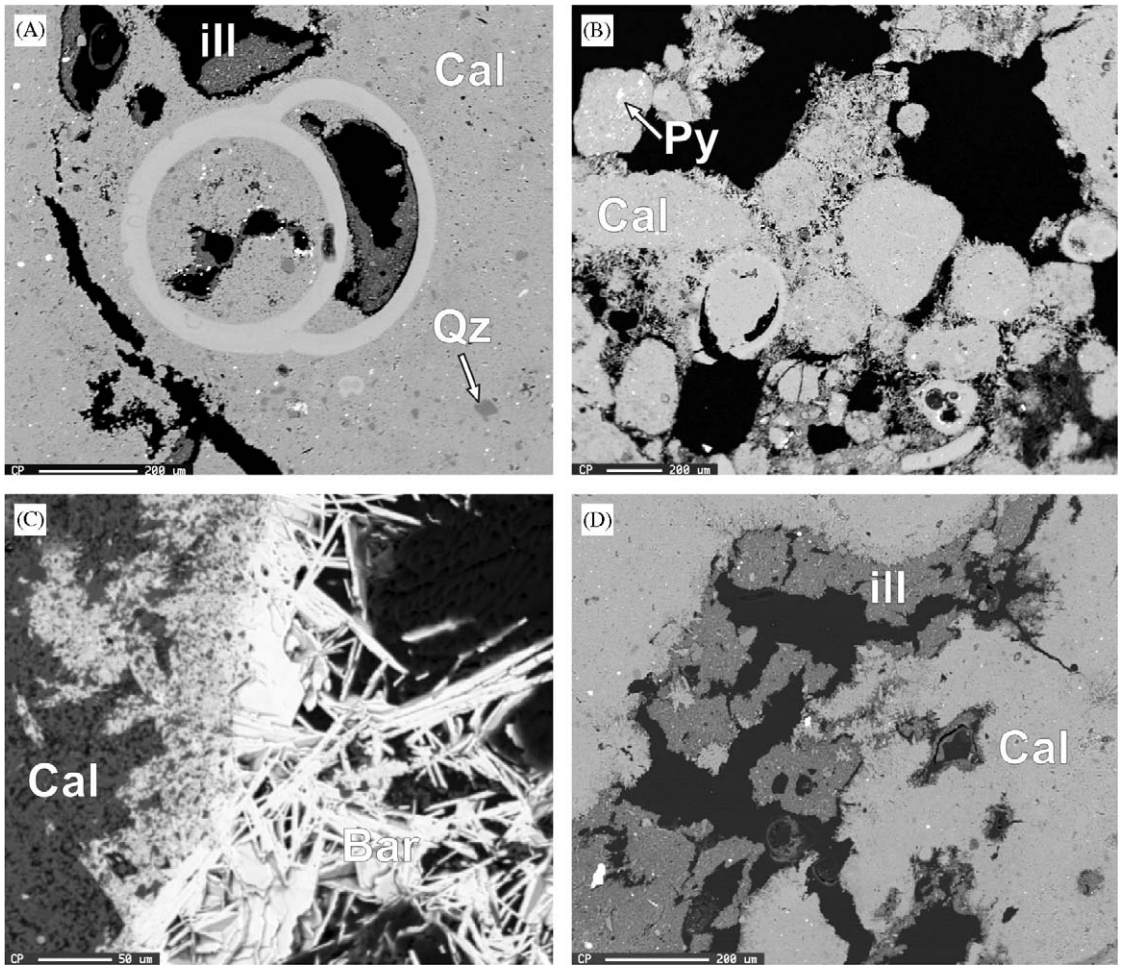

Fig. 9. SEM-BSE images of thin sections of authigenic carbonates from hydrocarbon seeps in the Gulf of Mexico. Bar, barite; Cal, calcite; ill, illite-like clay mineral; Qz, quartz; Py, pyrite. (A) Foraminifer with intraparticle porosity embedded in a fine-grained matrix of high magnesium calcite and quartz. Carbonate concretions of the Green Canyon. (B) Foraminifera and mud intraclasts cemented by aragonite. Carbonate slabs of the Green Canyon. (C) Barite crystals from a carbonate slab of the Green Canyon. (D) Void partially filled by small acicular aragonite crystals followed by a groundmass of illite-like clay mineral. Wackestone from the Chapopote knoll.

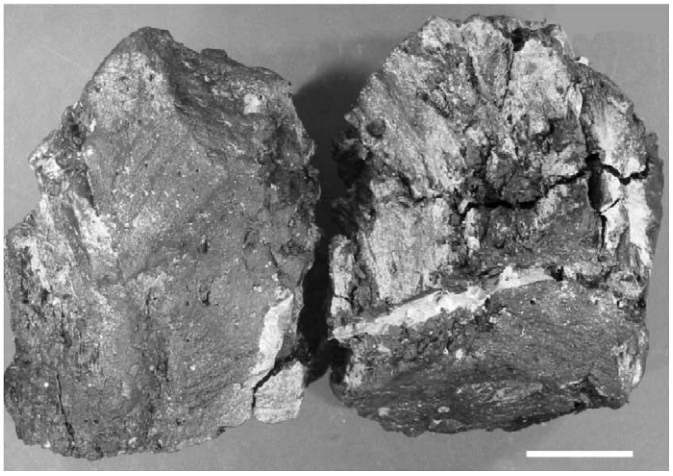

Fig. 10. Hand specimens of tar produced by asphalt volcanism at the Chapopote knoll. Bar scale: 5 cm.

The differences in shape and porosity reflect the different environment and formation conditions for the authigenic carbonate deposits. In the concretions of the Green Canyon, the channel macroporosity would serve as conduits of hydrocarbon seepage and could also represent casts of gas hydrates. Conversely, carbonate slabs develop pavements that cover the unconsolidated pelagic and hemipelagic mud in areas with diffuse methane seepage. According to Sassen et al. (1993, 2004), the occurrence of *Beggiatoa* mats that blanket seafloor sediments in cold seep areas obstructs the fluid flow between sediment and seawater, thereby promoting the microbial processes that trigger authigenic carbonate precipitation.

Consistent with their close association to slow seepage of viscose asphalt, the vug porosity of the authigenic carbonates of the Chapopote knoll is infilled by tar and oil. These carbonates are further distinguished by a greater

Table 1
Elemental composition (major and minor elements) of gas and oil seepage-related sediments

Sample	Location	SiO_2 (wt%)	TiO_2 (wt%)	Al_2O_3 (wt%)	Fe_2O_3 t (wt%)	MnO (wt%)	MgO (wt%)	CaO (wt%)	Na_2O (wt%)	K_2O (wt%)	SO_3 (wt%)	P_2O_5 (wt%)	LOI (wt%)	Total (wt%)
C-1[a]	Chapopote Hill	6.52	0.074	2.437	1.092	0.038	1.194	46.22	0.432	0.334	n.a.	0.041	41.8	100.1
C-2[a]	Green Canyon	12.06	0.144	3.927	1.312	0.14	3.546	42.21	0.384	0.764	n.a.	0.054	36.4	100.9
C-3[a]	Green Canyon	11.30	0.108	3.56	1.245	0.100	3.96	41.48	0.079	0.547	n.a.	0.066	39.8	102.2
C-4[a]	Green Canyon	9.86	0.092	2.96	1.1	0.059	3.92	42.95	0.346	0.445	n.a.	0.046	38.4	100.2
C-5[a]	Green Canyon	12.12	0.114	3.58	1.46	0.143	3.42	41.2	0.098	0.54	n.a.	0.057	37.7	100.4
C-7[a]	Green Canyon	13.54	0.14	3.55	1.34	0.125	4.25	40.68	0.37	0.78	n.a.	0.071	35.7	100.5
S-1[b]	Green Canyon	51.53	0.599	14.94	5.36	0.097	2.6	3.37	2.28	2.57	n.a.	0.024	16.9	100.27
S-2[a]	Green Canyon	13.63	0.143	4.36	3.36	0.167	3.41	36.61	0.416	0.689	3.28	0.13	32.7	95.62

		Rb (ppm)	Sr (ppm)	Ba (ppm)	Y (ppm)	Zr (ppm)	Nb (ppm)	V (ppm)	Cr (ppm)	Co (ppm)	Ni (ppm)	Cu (ppm)	Zn (ppm)	Th (ppm)	Pb (ppm)
C-1[a]	Chapopote Hill	11	4432	33	<0.5	29	<0.7	39	23	<3	10	41	15	4	<5
C-2[a]	Green Canyon	27	813	246	4	26	1	37	17	5	6	19	19	<3	5
C-3[a]	Green Canyon	16	849	280	2	24	<0.7	34	11	3	4	17	15	<3	<5
C-4[a]	Green Canyon	20	1031	239	2	22	1	44	16	6	5	20	21	<3	<5
C-5[a]	Green Canyon	21	900	268	4	28	1	49	15	5	4	22	22	<3	<5
C-7[a]	Green Canyon	27	873	276	4	33	3	34	15	6	8	21	21	5	5
S-1[b]	Green Canyon	92	125	434	25	143	9	220	96	14	43	35	91	12	15
S-2[a]	Green Canyon	25	1104	4091	4	29	1	50	20	8	15	14	26	<3	<5

LOI = lost on ignition; n.a. = not analyzed.
[a]Authigenic carbonates.
[b]Mud.

Table 2
Carbon and oxygen isotopic analyses of carbonate deposits related to gas and oil seepage in the Gulf of Mexico

Sample		Location	Description	$\delta^{13}C_{vpdb}$	$\delta^{18}O_{vpdb}$
C1-a	a	Chapopote knoll	Bivalve shell	−3.7	4.3
C1-b	b		Wackestone micrite	−23.0	4.1
C1-c	c		Wackestone micrite	−23.5	4.4
C2-a	a	Green Canyon	Mudstone micrite	−31.6	3.4
C2-b	b		Mudstone micrite	−30.3	3.9
C2-c	c		Mudstone micrite	−28.7	4.2
C2-d	d		Mudstone micrite	−27.8	4.1
C2-e	e		Mudstone micrite	−28.0	4.0
C5-a	a		Mudstone micrite	−30.9	4.3
C5-b	b		Mudstone micrite	−33.0	4.3
C7	a		Mudstone micrite	−36.9	3.7
C7	b		Mudstone micrite	−27.7	3.9
S2-a	a		Mudstone micrite	−36.8	4.4
S2-b	b		Mudstone micrite	−28.8	4.1

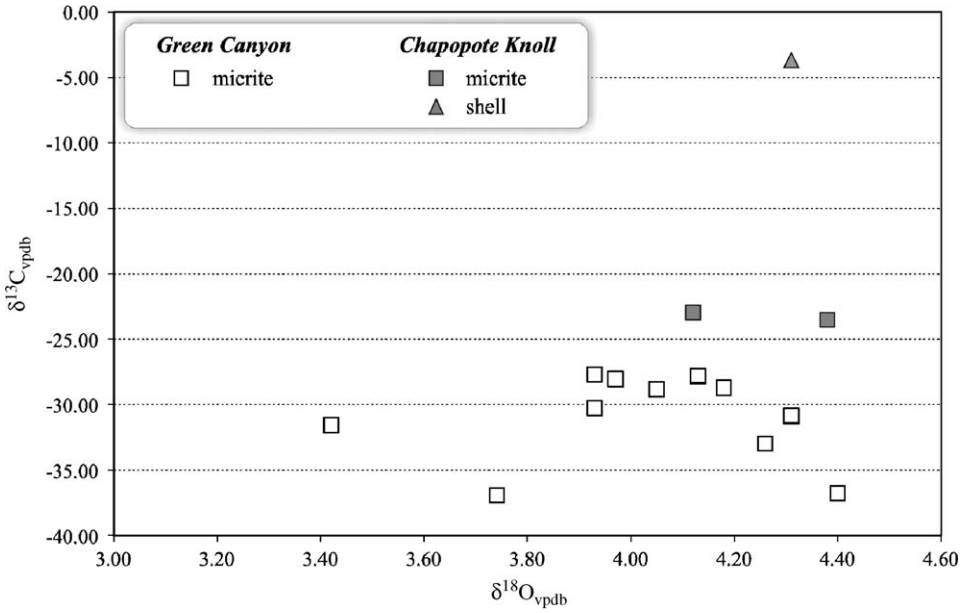

Fig. 11. Plot of carbon and oxygen stable isotope composition of authigenic carbonates related to the two seep locations studied in the Gulf of Mexico.

abundance of bivalve shell allochems per the abundant benthic cold-seep fauna that colonize the tar outcrops (MacDonald et al., 2004). This feature suggests that they formed through a lithification of the top few millimeters of the seabed sediments.

8.2. Mineralogy, carbon and oxygen isotopes and carbonate formation

High-Mg calcite is the main component of the fine-grained matrix of the authigenic carbonates of the cold seeps of the Green Canyon. Similarly, it is the main mineral in authigenic deposits that occur in relation to methane seepage in the areas of the Mediterranean (Aloisi et al., 2000), the Oregon/Washington margin (Ritger et al., 1987) and Baffin Island (Matsumoto, 1990). High-Mg calcite precipitates under the same conditions as aragonite (high SO_4^{2-} concentration and Mg^{2+}/Ca^{2+} ratio) and, according to Aloisi et al. (2000), the source of magnesium in methane-derived carbonates can be (1) rising cold seep fluids or (2) bottom seawater. In the Chapopote knoll samples, the main carbonate is low-Mg calcite, suggesting that the environment fluids have lower Mg^{2+}/Ca^{2+} ratios.

The $\delta^{13}C$ analyzed on the fine-grained matrix of the authigenic carbonates delivers values as low as −36.9‰. Authigenic carbonate rocks depleted in ^{13}C are a common feature of the cold seeps of the GOM (Sassen et al., 2004). According to Cavagna et al. (1999), a strong depletion in ^{13}C in carbonates ($\delta^{13}C$ values between −25 and −50‰) is proof of a methane-related origin. At cold seeps, microbial anaerobic oxidation of methane produces carbonate species that are incorporated into the carbonate lattice

(Ritger et al., 1987). This process of carbonate precipitation caused by microbial methanotrophic activity has been widely reported from cold seeps elsewhere (e.g., Cavagna et al., 1999; Aloisi et al., 2000; Boetius et al., 2000; Peckmann et al., 2001; Greinert et al., 2002; Chen et al., 2005), including the GOM (e.g., Formolo et al., 2004; Sassen et al., 2004) and in methane-rich hydrothermal vents (Canet et al., 2003). Methane oxidation by anaerobic methanotrophic communities has also been demonstrated in the deep hydrothermal vents at Guaymas Basin (Teske et al., 2002).

According to Sassen et al. (1993, 2004), the occurrence of *Beggiatoa* mats covering the seafloor sediments at the cold seeps of the GOM obstructs the fluid flow between the water-sediment interface and favors the microbial methane oxidation that enhances authigenic carbonate precipitation. This enables anaerobic methane oxidation in spite of the prevalent oxidizing conditions of the bottom seawater of the GOM as reported by Bohrmann and Schenck (2004).

In cold seeps, seawater sulfate reduction coupled with anaerobic methane oxidation concurrently triggers sulfide formation and carbonate precipitation (Kohn et al., 1998). Having been related to the activity of chemosynthetic microbial communities, these processes can be summarized with the following chemical reaction (e.g., Aloisi et al., 2000; Valentine and Reeburgh, 2000):

$$CH_4 + SO_4^{2-} \rightarrow (HCO_3)^- + HS^- + H_2O.$$

The precipitation of calcium carbonates takes place as a consequence of an increase in carbonate alkalinity whereby HS^- reacts with iron from the detrital sediments to produce pyrite (Peckmann et al., 2001).

In all of the studied authigenic carbonates, pyrite occurs disseminated and in the form of framboidal aggregates (Fig. 6D) in agreement with a prevalence of microbially triggered reactions of methane oxidation and sulfate reduction. The textures of pyrite (framboids) are consistent with precipitation related to biological activity. Though pyrite framboids have been associated with biogenic deposition (e.g., Barriga, 1990), they can occasionally be produced by abiotic processes (Berner, 1969).

The $\delta^{18}O$ values of the analyzed authigenic carbonates vary in a narrow range around 4‰. The analyzed $\delta^{18}O$ values are very close to those obtained by Aloisi et al. (2000) in cold seep carbonates from the Mediterranean. The oxygen isotopic composition in carbonates depends upon the temperature and the $\delta^{18}O$ of the mineralizing fluids. According to the equilibrium calibrations established by O'Neil et al. (1969), the temperatures of crystallization range between 5 and 9 °C for the $\delta^{18}O$ values measured in the fine-grained carbonate matrix using a mean $\delta^{18}O$ of water of 2‰ corresponding to pore fluids in cold seeps of the GOM (Aharon and Fu, 2003). These temperatures agree with bottom seawater temperatures in the GOM (Bohrmann and Schenck, 2004) and with the presence of gas hydrates.

Barite is highly abundant in the carbonate slabs of the Green Canyon's cold seeps. This mineral has been reported in relation to modern seepage of hydrocarbon and barium rich cold fluids (e.g., Greinert et al., 2002; Torres et al., 2003). Accordingly to Torres et al. (2003), the ultimate source of barium in these cold seeps is the "biogenic" barite that precipitates from the water column in high productivity areas and accumulates in the pelagic sediments. Upon burial, sulfate consumption in pore fluids due to methane oxidation allows barite dissolution followed by barium remobilization upwards to the seafloor discharge areas. It re-precipitates there as it combines with sulfate from downwards diffusing seawater. The abundance of barite in the carbonate slabs of the Green Canyon agrees with its formation as pavements near the water–sediment interface. On the other hand, the lack of barite in the cold seeps of the Chapopote knoll samples could be attributed to an absence of previous "biogenic" accumulations in the underlying sediments.

9. Conclusions

Seafloor hydrocarbon seepage associated with persistent upward migration of oil and gas (cold seeps) in the GOM produces deposits of authigenic carbonate. These deposits consist in matrix-supported, oil-impregnated limestones made up of a fine-grained matrix of calcite that includes bioclasts in variable amounts. In the cold seeps of the Green Canyon on the Louisiana slope, authigenic carbonates form (1) concretions a few meters below the seafloor and (2) slabs that take the shape of hardground-like pavements near the water–sediment interface. These carbonates are mudstones featuring pelagic foraminifera included as allochems and a mud matrix composed of high-Mg calcite (up to 9.99% $MgCO_3$ molar), disseminated pyrite and barite crystals that occur as vug and crack lining. The carbonate concretions show channel macroporosity that characterizes conduits of hydrocarbon seepage and casts of gas hydrates.

In the Chapopote knoll area on the abyssal plain near the Campeche Bank, authigenic carbonates occur in relation to "rocky" outcrops of tar and form irregularly shaped crusts of wackestones with bivalve shell bioclasts and highly irregular vug porosity partly filled with tar. The mud matrix is composed of low-Mg calcite (up to 0.60% $MgCO_3$ molar) with disseminated pyrite and late aragonite cement partially lines the porosity walls and binds the allochems. The abundance of bivalve shell allochems suggests that the carbonate deposits formed from the lithification of the top few millimeters of the seabed sediments.

In all the samples, the authigenic carbonate mud shows a strong depletion in ^{13}C with respect to normal marine carbonates. This suggests a methane-related origin. Authigenic carbonates should precipitate as a consequence of a microbially mediated reaction of anaerobic methane oxidation coupled with seawater sulfate reduction. This origin agrees with the occurrence of disseminated pyrite crystals.

The $\delta^{18}O$ values in the carbonate mud of all the analyzed samples are in agreement with a precipitation from pore

waters slightly enriched in ^{18}O at a range of temperatures between 5 and 9 °C.

Barite is very abundant in the carbonate slabs of the Green Canyon's cold seeps. Its precipitation can be attributed to expelled barium-rich, sulfate-free cold seep fluids reacting with sulfate-rich, downwards-diffusing seawater. This process agrees with its occurrence in the authigenic carbonate pavements that form near the water–sediment interface.

The close relationship between authigenic carbonates and methane seepage has been considered a valid criterion for submarine hydrocarbon exploration (Chen et al., 2005; Pacheco-Muñoz et al., 2005). Therefore, the petrographic and geochemical characterization of authigenic carbonates may soon provide information leading to the discovery of new hydrocarbon reserves.

Acknowledgments

Mexican funding was provided by the UNAM projects IN107003 and IN114602. In addition, this research was funded by: BMBF Bonn, grant 03G0174A Geotechnology program to G. Bohrman RCOM, logistic support for joint German-US-Mexican cruise to explore the Gulf of Mexico Outer Continental Slope NOAA to I. MacDonald, TAMU-CC, SEP-CONACyT 40158 & PAPIIT IN224503 to E. Escobar, ICML UNAM. Sampling was carried out during the SO174 (OTEGA-II) cruise of the German research vessel SONNE, sponsored by German projects LOTUS, OMEGA and MUMM. We thank the scientific team and crew of the SONNE for their work during the cruise.

We thank M. Reyes Salas and S. Ángeles García for their assistance during the SEM analyses. The authors thank I. Villagrana for his help during FRX analyses and assistance in XRD. Thanks also go to A. Camprubí and S.I. Franco for their comments and to D.G. Roberts, R. van Blokland and B. Martiny for reviewing the manuscript.

References

Aharon, P., Fu, B.S., 2000. Microbial sulfate reduction rates and sulfur and oxygen isotope fractionations at oil and gas seeps in deepwater Gulf of Mexico. Geochimica et Cosmochimica Acta 64, 233–246.

Aharon, P., Fu, B., 2003. Sulfur and oxygen isotopes of coeval sulfate–sulfide in pore fluids of cold seep sediments with sharp redox gradients. Chemical Geology 142, 1–18.

Aloisi, G., Pierre, C., Rouchy, J.M., Foucher, J.P., Woodside, J., 2000. Methane-related authigenic carbonates of eastern Mediterranean Sea mud volcanoes and their possible relation to gas hydrate destabilisation. Earth and Planetary Science Letters 184, 321–338.

Aloisi, G., Wallmann, K., Bollwerk, S.M., Derkachev, A., Bohrmann, G., Suess, E., 2004. The effect of dissolved barium on biogeochemical processes at cold seeps. Geochimica et Cosmochimica Acta 68, 1735–1748.

Antoine, J.W., 1972. Structure of the Gulf of Mexico. In: Rezak, R., Henry, V.J. (Eds.), Contributions on the Geological and Geophysical Oceanography of the Gulf of Mexico. Texas A&M University Oceanographic Studies 3, Gulf Publishing Company, Houston, USA, 303p.

Arvidson, R.S., Morse, J.W., Joye, S.B., 2004. The sulfur biogeochemistry of chemosynthetic cold seep communities, Gulf of Mexico, USA. Marine Chemistry 87, 97–119.

Ashi, J., Tokuyama, H., Taira, A., 2002. Distribution of methane hydrate BSRs and its implication for the prism growth in the Nankai Trough. Marine Geology 187, 177–191.

Barriga, F.J.A.S., 1990. Metallogenesis in the Iberian Pyrite Belt. In: Dallmeyer, R.D., Martinez, E. (Eds.), Geology of Hercynian Iberia. Springer, Berlin, pp. 369–379.

Berner, R.A., 1969. The synthesis of framboidal pyrite. Economic Geology 64, 383–384.

Boetius, A., Ravenschlag, K., Schubert, C., Rickert, D., Widdel, F., Gieseke, A., Amann, R., Jørgensen, B.B., Witte, U., Pfannkuche, O., 2000. A marine microbial consortium apparently mediating anaerobic oxidation of methane. Nature 407, 623–626.

Bohrmann, G., Schenck, S., 2004. RV SONNE cruise report SO174, OTEGA II, Balboa—Corpus Christi—Miami (1 October—12 November, 2003). GEOMAR Report 117, Kiel, Germany, 130pp.

Bryant, W.R., Lugo, J., Cordova, C., Salvador, A., 1991. Physiography and bathymetry. In: Salvador, A. (Ed.), The Gulf of Mexico Basin, The Geology of North America, vol. J, no.14. Geological Society of America, Boulder, CO, pp. 13–30.

Canet, C., Prol-Ledesma, R.M., Melgarejo, J.C., Reyes, A., 2003. Methane-related carbonates formed at submarine hydrothermal springs: a new setting for microbially-derived carbonates? Marine Geology 199, 245–261.

Cavagna, S., Clari, P., Martire, L., 1999. The role of bacteria in the formation of cold seep carbonates: geological evidence from "Montferrato" (Tertiary, NW Italy). Sedimentary Geology 126, 253–270.

Chen, D.F., Huang, Y.Y., Yuan, X.L., Cathles III, L.M., 2005. Seep carbonates and preserved methane oxidizing archaea and sulfate reducing bacteria fossils suggest recent gas venting on the seafloor in the Northeastern South China Sea. Marine and Petroleum Geology 22, 613–621.

Collett, T.S., Kuuskraa, V.A., 1998. Hydrates contain vast world gas resources. Oil and Gas Journal 96, 90–95.

Coplen, T., 1988. Normalization of oxygen and hydrogen isotope data. Chemical Geology 72, 293–297.

Dunham, R.J., 1962. Classification of carbonate rocks according to depositional texture. In: Ham, W.E. (Ed.), Classification of Carbonate Rocks. American Association Of Petroleum Geologists Memoir, vol. 1, pp. 108–121.

Emsbo, P., Johnson, C.A., 2004. Formation of modern and Paleozoic stratiform barite at cold methane seeps on continental margins: comment and reply. Geology: Online Forum, e64.

Ewing, M., Antoine, J., 1966. New seismic data concerning sediments and diapiric structures in Sigsbee Deep and upper continental slope, Gulf of Mexico. AAPG Bulletin 50, 479–504.

Fisher, C.R., MacDonald, I.R., Sassen, R., Young, C.M., Macko, S.A., Hourdez, S., Carney, R.S., Joye, S., McMullin, E., 2000. Methane ice worms: Hesiocaeca Colonizing fossil fuel reserves. Naturwissenschaften 87, 84–187.

Formolo, M.J., Lyons, T.W., Zhang, C., Kelley, C., Sassen, R., Horita, J., Cole, D.R., 2004. Quantifying carbon sources in the formation of authigenic carbonates at gas hydrate sites in the Gulf of Mexico. Chemical Geology 205, 253–264.

Gómez-Pérez, I., 2003. An Early Jurassic deep-water stromatolitic bioherm related to possible methane seepage (Los Molles Formation, Neuquén, Argentina). Palaeogeography, Palaeoclimatology, Palaeoecology 201, 21–49.

Greinert, J., Bollwerk, S.M., Derkachev, A., Bohrmann, G., Suess, E., 2002. Massive barite deposits and carbonate mineralization in the Derugin Basin, Sea of Okhotsk: precipitation processes at cold seep sites. Earth and Planetary Science Letters 203, 165–180.

Han, X., Suess, E., Sahling, H., Wallmann, K., 2004. Fluid venting activity on the Costa Rica margin: new results from authigenic carbonates. International Journal of Earth Science (Geol. Rundsch) 93, 596–611.

Hovland, M., Judd, A., 1988. Seabed Pockmarks and Seepages. Impact on Geology, Biology and the Marine Environment. Graham & Trotman, London, UK, 296pp.

Joye, S.B., Boetius, A., Orcutta, B.N., Montoya, J.P., 2004. The anaerobic oxidation of methane and sulfate reduction in sediments from Gulf of Mexico cold seeps. Chemical Geology 205, 219–238.

Judd, A., Davies, G., Wilson, J., Holmes, R., Baron, G., Bryden, I., 1997. Contributions to atmospheric methane by natural seepages on the UK continental shelf. Marine Geology 140, 427–455.

Kohn, M.J., Riciputi, L.R., Stakes, D., Orange, D.L., 1998. Sulfur isotope variability in biogenic pyrite: Reflections of heterogeneous bacterial colonization? American Mineralogist 83, 1454–1468.

Lance, S., Henry, P., Le Pichon, X., Lallemant, S., Chamley, H., Rostek, F., Faugères, J.C., Gonthier, E., Olu, K., 1998. Submersible study of mud volcanoes seaward of the Barbados accretionary wedge: sedimentology, structure and rheology. Marine Geology 145, 255–292.

Lozano-Santa Cruz, R., Verma, S.P., Girón, P., Velasco, F., Morán, D., Viera, F., Chávez, G., 1995. Calibración preliminar de fluorescencia de rayos X para análisis cuantitativo de elementos mayores en rocas ígneas. Actas INAGEQ 1, 203–208.

Luff, R., Wallmann, K., Aloisi, G., 2004. Numerical modeling of carbonate crust formation at cold vent sites: significance for fluid and methane budgets and chemosynthetic biological communities. Earth and Planetary Science Letters 221, 337–353.

MacDonald, I.R., Sager, W.W., Peccini, M.B., 2003. Gas hydrate and chemosynthetic biota in mounded bathymetry at mid-slope hydrocarbon seeps: Northern Gulf of Mexico. Marine Geology 198, 133–158.

MacDonald, I.R., Bohrmann, G., Escobar, E., Abegg, F., Blanchon, P., Blinova, V., Brückmann, W., Drews, M., Eisenhauer, A., Han, X., Heeschen, K., Meier, F., Mortera, C., Naehr, T., Orcutt, B., Bernard, B., Brooks, J., de Farago, M., 2004. Asphalt volcanism and chemosynthetic life in the Campeche Knolls, Gulf of Mexico. Science 304, 999–1002.

Macgregor, D., 1993. Relationships between seepage, tectonics and subsurface petroleum reserves. Marine and Petroleum Geology 10, 606–619.

Matsumoto, R., 1990. Vuggy carbonate crusts formed by hydrocarbon seepage on the continental shelf of Baffin Island, northeast Canada. Geochemical Journal 24, 143–158.

Michaelis, W., Seifert, R., Nauhaus, K., Treude, T., Thiel, V., Blumenberg, M., Knittel, K., Gieseke, A., Peterknecht, K., Pape, T., Boetius, A., Amann, R., Jorgensen, B.B., Widdel, F., Peckmann, J., Pimenov, N.V., Gulin, M.B., 2002. Microbial reefs in the Black Sea fueled by anaerobic oxidation of methane. Science 297, 1013–1015.

Milkov, A.V., 2004. Global estimates of hydrate-bound gas in marine sediments: how much is really out there? Earth Science Reviews 66, 183–197.

Milkov, A.V., Vogt, P.R., Crane, K., Lein, A.Y., Sassen, R., Cherkashev, G.A., 2004. Geological, geochemical, and microbial processes at the hydrate-bearing Håkon Mosby mud volcano: a review. Chemical Geology 205, 347–366.

Morán-Zenteno, D.J., 1984. Geology of the Mexican Republic. Studies in Geology, vol. 39. American Association of Petroleum Geologists, Tulsa, OH, 160p.

O'Neil, J.R., Clayton, R.N., Mayeda, T.K., 1969. Oxygen isotope fractionation in divalent metal carbonates. Journal of Chemical Physics 51, 5547–5558.

Pacheco-Muñoz, J., Limón-González, M., Ortega-González, J.V., 2005. Exploración geoquímica de superficie del fondo marino (EGS) en el Golfo de México (1998–2004). XV Congreso Nacional de Geoquímica, San Luis Potosí, México, Actas INAGEQ 11, pp. 94–97.

Paytan, A., Mearon, S., Cobb, K., Kastner, M., 2002. Origin of marine barite deposits: Sr and S isotope characterization. Geology 30, 747–750.

Peckmann, J., Thiel, V., 2004. Carbon cycling at ancient methane seeps. Chemical Geology 205, 443–467.

Peckmann, J., Reimer, A., Luth, U., Luth, C., Hansen, B.T., Heinicke, C., Hoefs, J., Reitner, J., 2001. Methane-derived carbonates and authigenic pyrite from the northwestern Black Sea. Marine Geology 177, 129–150.

Pindell, J.L., 1985. Alleghenian reconstruction and subsequent evolution of the Gulf of Mexico, Bahamas, and Proto-Caribben. Tectonics 4, 1–39.

Pinheiro, L.M., Ivanov, M.K., Sautkin, A., Akhmanov, G., Magalhães, V.H., Volkonskaya, A., Monteiro, J.H., Somoza, L., Gardner, J., Hamouni, N., Cunha, M.R., 2003. Mud volcanism in the Gulf of Cadiz: results from the TTR-10 cruise. Marine Geology 195, 131–151.

Ritger, S., Carson, B., Suess, E., 1987. Methane-derived authigenic carbonates formed by subduction-induced pore-water expulsion along the Oregon/Washington margin. Geological Society of America Bulletin 98, 147–156.

Roberts, H.H., McBride, R.A., Coleman, J.M., 1999. Outer shelf and slope geology of the Gulf of Mexico: an overview. In: Kumpf, H., Steidinger, K., Sherman, K. (Eds.), The Gulf of Mexico Large Marine Ecosystem. Blackwell Science, USA, 704p.

Salas de León, D.A., Monreal-Gómez, M.A., 1997. Circulación y estructura termohalina del Golfo de México. Contribuciones a la oceanografía física en México. Unión Geofísica Mexicana, monografía no. 3.

Salvador, A., 1987. Late Triassic–Jurassic paleogeography and origin of Gulf of Mexico basin. AAPG Bulletin 71, 419–451.

Sassen, R., Roberts, H.H., Aharon, A., Larkin, J., Chinn, E.W., Carney, R., 1993. Chemosynthetic bacterial mats at cold hydrocarbon seeps. Gulf of Mexico continental slope. Organic Geochemistry 20, 77–89.

Sassen, R., Losh, S.L., Cathles III, L., Roberts, H.H., Whelan, J.K., Milkov, A.V., Sweet, S.T., DeFreitas, D.A., 2001. Massive vein-filling gas hydrate: relation to ongoing gas migration from the deep subsurface in the Gulf of Mexico. Marine and Petroleum Geology 18, 551–560.

Sassen, R., Roberts, H.H., Carney, R., Milkov, A.V., DeFreitas, D.A., Lanoil, B., Zhang, C., 2004. Free hydrocarbon gas, gas hydrate, and authigenic minerals in chemosynthetic communities of the northern Gulf of Mexico continental slope: relation to microbial processes. Chemical Geology 205, 195–217.

Schmidt, M., Botz, R., Winn, K., Stoffers, P., Thiessen, O., Herzig, P., 2002. Seeping hydrocarbons and related carbonate mineralisations in sediments south of Lihir Island (New Ireland fore arc basin, Papua New Guinea). Chemical Geology 186, 249–264.

Stakes, D.S., Orange, D., Paduan, J.B., Salamy, K.A., Maher, N., 1999. Cold-seeps and authigenic carbonate formation in Monterey Bay, California. Marine Geology 159, 93–109.

Suess, E., Torres, M.E., Bohrmann, G., Collier, R.W., Greinert, J., Linke, P., Rehder, G., Trehu, A., Wallmann, K., Winckler, G., Zuelger, E., 1999. Gas hydrate destabilization: enhanced dewatering, benthic material turnover and large methane plumes at the Cascadia convergent margin. Earth and Planetary Science Letters 170, 1–15.

Teske, A., Hinrichs, K.-U., Edgcomb, V., de Vera Gómez, A., Kysela, D., Sylva, S.P., Sogin, M.L., Jannasch, H.W., 2002. Microbial diversity of hydrothermal sediments in the Guaymas Basin: evidence for anaerobic methanotrophic communities. Applied and Environmental Microbiology 68-4, 1994–2007.

Tomczak, M., Godfrey, J.S., 1994. Regional Oceanography: An Introduction. Pergamon, Oxford, UK, 442pp.

Torres, M.E., Bohrmann, G., Dubé, T.E., Poole, F.G., 2003. Formation of modern and Paleozoic stratiform barite at cold methane seeps on continental margins. Geology 31, 897–900.

Valentine, D.L., Reeburgh, W.S., 2000. New perspectives on anaerobic methane oxidation. Environmental Microbiology 2, 477–484.

Wallmann, K., Linke, P., Suess, E., Bohrmann, G., Sahling, H., Schlüter, M., Dählmann, A., Lammers, S., Greinert, J., von Mirbach, N., 1997. Quantifying fluid flow, solute mixing, and biogeochemical turnover at cold vents of the eastern Aleutian subduction zone. Geochimica et Cosmochimica Acta 61, 5209–5219.

Watkins, J.S., Macrae, G., 1995. Bipolar simple-shear rifting responsible for distribution of mega-salt basins in Gulf of Mexico? In: Travis, C.J., et al. (Eds.), Gulf Coast Section SEPM Foundation Sixteenth Annual Research Conference, Program with Papers, pp. 297–305.